

Holonomic multi-controlled gates for single-photon states

Carlo Danieli,^{1,2,*} Valentina Brosco,¹ Claudio Conti,^{3,4} and Laura Pilozzi^{1,4}

¹*Institute for Complex Systems, National Research Council (ISC-CNR), Via dei Taurini 19, 00185 Rome, Italy*

²*Department of Physics and Astronomy, University of Florence, I-50019 Sesto Fiorentino, Italy*

³*Department of Physics, University of Sapienza, Piazzale Aldo Moro 5, 00185 Rome, Italy*

⁴*Research Center Enrico Fermi, Via Panisperna 89a, 00184 Rome, Italy*

(Dated: December 25, 2025)

Controlled and multi-controlled quantum gates, whose action on a target qubit depends on the state of multiple control qubits, represent a fundamental logical building block for complex quantum algorithms. We propose a scheme for realizing this class of gates based on non-Abelian holonomies in modulated photonic waveguide networks. Our approach relies on linear photonic circuits formed by two star networks coupled via a two-path circuit. A star network with M peripheral waveguides coupled to a single central site, or M -pod, naturally generalizes the tripod structure used in non-Abelian Thouless pumping and stimulated Raman adiabatic passage (STIRAP). In the present work, we first analyze the minimal case of two connected tripods and design adiabatic driving loops that implement single-qubit, CNOT, and SWAP gates. We then show how extending the approach to larger M -pod structures enables the realization of multiply controlled operations, which we exemplify by designing Toffoli and the OR gate on two coupled pentapods. Finally, we demonstrate that networks of connected tripods can implement the Deutsch quantum query algorithm.

I. INTRODUCTION

Non-Abelian holonomies [1, 2] represent the natural $U(N)$ generalization of Berry's geometric phase [3]. They were originally introduced by Wilczek and Zee in their seminal work [1], which elucidated the relation between non-Abelian gauge theories and the geometric structure of Hilbert space emerging in the adiabatic evolution of quantum systems with degenerate energy levels. Since then various experiments generated and detected non-Abelian holonomies in photonic platforms [4, 5], acoustic waveguides [6], quantum optical setups [7, 8], cold atoms [9], and superconducting devices [10]. At the same time, theoretical works highlighted their fundamental role in modeling quantum transport [11–14] and describing topological phenomena [15–17].

The basic relevance of non-Abelian holonomies is closely intertwined with their practical interest in quantum control [18–20] and quantum computing [21, 22]. In particular, as first demonstrated by Zanardi and Rasetti, holonomies can be exploited to implement a universal set of *holonomic quantum gates* (HQGs) [21]. This idea, introduced in Ref. [21], is based on encoding qubits in the eigenstates of a degenerate Hamiltonian H and performing unitary operations through the Wilczek–Zee holonomy by adiabatically modulating a set of classical control parameters defining H . A key advantage of HQGs lies in their robustness against certain kinds of noise and decoherence [23–26]. Since the pioneering work of Ref. [21], HQGs have been both theoretically proposed and experimentally realized across various physical platforms [27–32]. Furthermore, the potentially crucial role of HQGs in enabling more robust quantum computing architec-

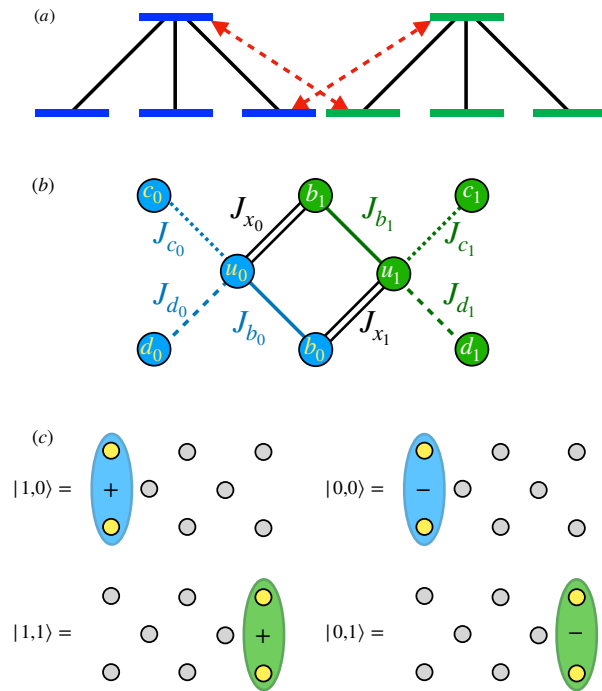


FIG. 1. (a) Scheme describing the structure of the Hamiltonian of two-coupled tripods. (b) Schematic of the array composed of two tripods respectively colored in blue and green. The two tripods are connected via the hopping J_{x_0} and J_{x_1} . (c) Two qubits encoding states $|s, p\rangle$ for the target qubit $p = 0$ (upper row) and $p = 1$ (lower row). At the initial parameters $J_{\ell_p} = 0$ for $\ell = c, d, x$ and $J_{b_p} = J$ for $p = 0, 1$ of the driving cycle, the states correspond to the four zero-energy degenerate eigenstates.

tures [33–37] has motivated various works aimed at realizing holonomic gates beyond the adiabatic regime [38–42].

* carlo.danieli@cnr.it

In both photonic and atomic implementations of holonomic systems, a crucial role is played by Hamiltonians with a tripod structure, such as those illustrated in Fig. 1(a). This type of Hamiltonian exhibits two degenerate energy levels for any value of the coupling parameters, and the holonomy is typically generated by adiabatically controlling these couplings. Hamiltonians of this kind lie at the heart of non-Abelian Thouless pumping [13] and stimulated Raman adiabatic passage (STIRAP) protocols [8, 18, 22, 42–45].

In this work, we go beyond standard single-qubit holonomic protocols, by focusing on the design of multi-controlled holonomic gates with m control qubits and one target qubit within an adiabatically modulated array of $2(2^m + 2)$ optical waveguides. This array consists of two coupled M -pods, each having $M = 2^m + 1$ legs connected to a central waveguide.

The system proposed in the present work encodes information in the state of a single-photon in a multimode setup and uses holonomies to manipulate this information implementing an holonomic version of linear optic quantum computing protocols[46–48].

In the simplest case, the array structure is based on two tripods, ($m = 1$), connected via hoppings that preserve the four-fold degeneracy of the single-photon space for any coupling strength as shown in Fig. 1(b). By properly choosing the qubit encoding scheme and the driving cycles, we engineer a universal set of holonomic transformations [49–52]. In particular, beside single-qubit operations, such as Hadamard and phase gates, we design controlled two-qubit gates, of the form $C_U = |0\rangle\langle 0| \otimes \mathbb{I} + |1\rangle\langle 1| \otimes U$ and the SWAP gate [53].

Multi-controlled quantum gates based on two coupled M -pods extend the CNOT by applying a gate U to a target qubit p conditioned on the state of m control qubits. These gates represent a basic logical building block in the design of complex quantum algorithms, see e.g. Refs.[54–57]. Here we encode the qubits in single-photon states on two coupled M -pods and we engineer driving protocols to control holonomically the evolution of the qubit states. As specific examples we propose the realization of the Toffoli gate [58] and the quantum OR gate on a structure formed by two coupled 5-pods which we call pentapods. Eventually we show that similar structures can be used to implement the Deutsch quantum query algorithm [59, 60].

II. PHOTONIC LATTICE AND QUBIT ENCODING

We consider a chiral symmetric photonic lattice of eight waveguides coupled through evanescent hoppings J_{i_p} with $i = b, c, d, x$, and $p = 0, 1$ shown in Fig. 1(b). The lattice consists of two tripods, colored in blue and green, connected via the hoppings J_{x_0} and J_{x_1} .

The dynamics of photon propagation is described by

a Schrödinger equation $i\partial_z|\psi(z)\rangle = H(z)|\psi(z)\rangle$ with Hamiltonian

$$H = H_0 + H_1 + H_X \quad (1)$$

where the 0,1 tripod Hamiltonian are given by $H_p = (J_{b_p}b_p^\dagger u_p + J_{c_p}c_p^\dagger u_p + J_{d_p}d_p^\dagger u_p + \text{H.c.})$ with $p = 0, 1$, while H_X denotes the coupling between the two tripods $H_X = (J_{x_0}b_1^\dagger u_0 + J_{x_1}b_0^\dagger u_1 + \text{H.c.})$. Chirality ensures that, for any choice of the hopping parameters, the spectrum of H consists of four degenerate modes $\mathcal{B} = \{|\psi_1\rangle, \dots, |\psi_4\rangle\}$ at energy $E_0 = 0$ and four non-degenerate non-zero modes. Chirality furthermore enforces that the zero modes lie only on the majority sublattice $\mathcal{M} = \{b_p, c_p, d_p\}_{p=0,1}$ – i.e. they are zero on the minority sublattice $m = \{u_p\}_{p=0,1}$ [61].

We focus on holonomic gates obtained by periodic and adiabatic modulation of the couplings along z i.e. the propagation distance along the waveguides, which plays the role of time in the evolution process. At $z = 0$ only J_{b_0} and J_{b_1} are different from zero while all other couplings vanish. In this initial configuration, the four orthonormal zero modes shown in Fig. 1(c), are

$$\begin{aligned} |\psi_1(0)\rangle &= \frac{|c_0\rangle - |d_0\rangle}{\sqrt{2}} & |\psi_2(0)\rangle &= \frac{|c_1\rangle - |d_1\rangle}{\sqrt{2}} \\ |\psi_3(0)\rangle &= \frac{|c_0\rangle + |d_0\rangle}{\sqrt{2}} & |\psi_4(0)\rangle &= \frac{|c_1\rangle + |d_1\rangle}{\sqrt{2}} \end{aligned} \quad (2)$$

yielding a natural encoding for two qubits in a single photon excitation. We can therefore recast the logic states in Eq. (2) as

$$\frac{|c_p\rangle + (2s-1)|d_p\rangle}{\sqrt{2}} \equiv |s, p\rangle \quad (3)$$

with $p = 0, 1$ denoting the position and $s = 0, 1$ the symmetry. For the realization of controlled gates the position p is the *target* qubit, while s is the *control* qubit.

III. SINGLE AND TWO-QUBIT GATES

We focus on the implementation of geometric gates by initializing the system in the degenerate subspace of zero modes $|\psi(0)\rangle = \sum_\nu c_\nu|\psi_\nu(0)\rangle$ defined in Eq. (2) and by manipulating adiabatically the coupling of the Hamiltonian H along the z coordinate following a cycle γ . Over the cycle γ of duration λ , the input state $|\psi(0)\rangle$ transforms as

$$|\psi(\lambda)\rangle = W_\gamma(\lambda, 0)|\psi(0)\rangle, \quad (4)$$

where $W_\gamma(\lambda, 0) = P \exp \left[i \oint_\gamma \Gamma_z dz \right]$ indicates the $U(4)$ holonomy, P denotes the path-ordering and $[\Gamma_z]_{\nu\nu'} = \langle \psi_\nu | i\partial_z | \psi_{\nu'} \rangle$ is the Wilczek-Zee connection.

As first highlighted by Zanardi and Rasetti [21], non-Abelian holonomies can be exploited to implement a universal set gates. In particular, within the setup of

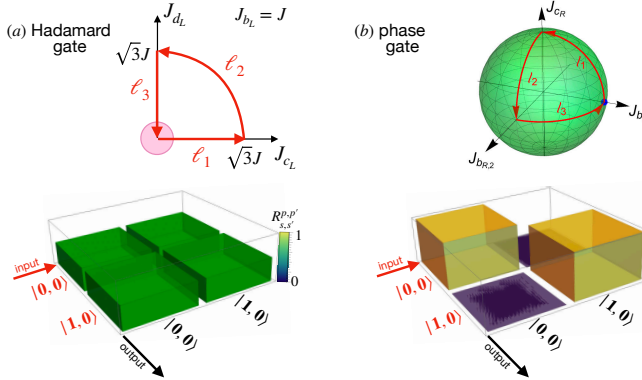


FIG. 2. (a) Driving cycle in the parameter space (the circle indicates the initial point) and quantum state tomography for the single qubit Hadamard gate. (b) Same as (a) for the single qubit phase gate.

Fig. 1(b), they allow for the implementation of rotations and phase gates acting on the symmetry quantum number s , respectively given by $V_\xi = e^{i\xi\sigma_y} \otimes \sigma_0$ and $V_\varphi = e^{i\frac{\varphi}{2}(\sigma_0 - \sigma_z)} \otimes \sigma_0$.

Both transformations can be generated holonomically through adiabatic manipulations acting on both tripods simultaneously and setting $H_T = 0$ following the route presented Refs [13, 44, 45] for single tripod systems.

For example modulating each tripod with the driving cycles shown in Fig. 2, one can realize the Hadamard gate and the phase gate, respectively – see Appendix B for more details. See Fig. 2(a,b) for the corresponding final state tomography, extracted from the numerical data as $R^{p,p'}_{s,s'} = |\langle s', p' | \psi_{s,p}(\lambda) \rangle|^2$.

For the four states system considered in this work, the holonomic evolution along suitably defined cycles also offers a natural playground to design two-qubit gates. We start by focusing on the generation of conditional gates of the form:

$$C_\eta = |0\rangle\langle 0| \otimes \mathbb{I} + |1\rangle\langle 1| \otimes U_\eta \quad (5)$$

where $U_\eta = e^{i\eta\sigma_y}$ is a rotation around the y -axis of the Bloch sphere and the angle η depends only the geometry of the cycle and the structure of the Hilbert space – see Appendix C for more details. An example is illustrated in Fig. 3 where we demonstrate a CNOT gate – *i.e.* a gate that swaps the target qubit p if and only if the control qubit s is $|1\rangle$. The latter corresponds to setting $\eta = \pi/2$ – hence, $U_\eta = i\sigma_y$ in Eq.(5).

In our photonic array, this gate is achieved holonomically by setting $J_{x_0} = J_{x_1} \equiv J_x$, $J_{b_0} = J_{b_1} \equiv J_b$ and $J_{c_p} = J_{d_p} \equiv J_c$ for both $p = 0, 1$. The symmetry relations for $J_{c_p} = J_{d_p}$ imply that $|0,0\rangle$ and $|0,1\rangle$ are exact eigenstates of the array along the whole cycle γ while the states $|1,0\rangle$ and $|1,1\rangle$ evolve adiabatically according to Eq.(4) leading $W_\gamma(\lambda, 0) = C_{\pi/2}$ – see Appendix C for more details.

In Fig. 3(c,d) we show the evolution of the states $|1,0\rangle$ and $|1,1\rangle$ obtained by numerically solving the

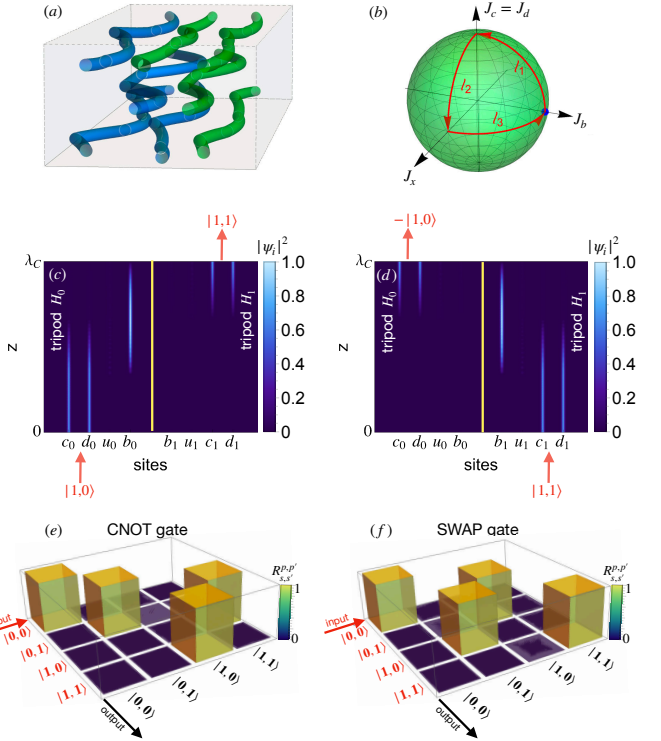


FIG. 3. (a) Illustration of the lattice pumped to implement a CNOT gate. The left tripod $p = 0$ is colored in green while the right tripod $p = 1$ is colored in blue. (b) Driving cycle in the parameter space. The circle indicates the initial point. (c,d) Propagation of $|1,0\rangle$ and $|1,1\rangle$ states respectively over one cycle period. The yellow lines separate the 0 and the 1 tripods. (e,f) Quantum state tomography for the CNOT gate and the SWAP gate respectively.

Schrödinger equation $i\partial_z|\psi(z)\rangle = H(z)|\psi(z)\rangle$. As predicted, the transformation flips the target qubit p while preserving their control qubit $s = 1$. In Fig. 3(e) we show the numerical quantum state tomography matrix R .

On the other hand, by setting $J_{c_1} = -J_{d_1}$ while keeping $J_{c_0} = J_{d_0}$ in the cycle in Fig. 3(b), the CNOT gate can be turned into a SWAP gate – see Appendix C for more details. This gate indeed, swaps the two qubits $|0,1\rangle$ and $|1,0\rangle$ while keeping $|0,0\rangle$ and $|1,1\rangle$ unchanged. The numerically computed quantum state tomography is shown in Fig. 3(f). This implementation of the SWAP gate requires changing the sign of the hopping J_{d_1} from positive to negative, which can be done experimentally by *e.g.* introducing an additional auxiliary waveguide between u_1 and d_1 [62, 63], through a resistor applied to array [64], or by replacing certain waveguide with multi-orbital ones [65, 66].

IV. MULTI-CONTROLLED GATES

The array shown in Fig. 1(b) can be modified to host multi-controlled gates by replacing the two tripods with two M -pods. An M -pod is a system of $M + 1$ waveguides

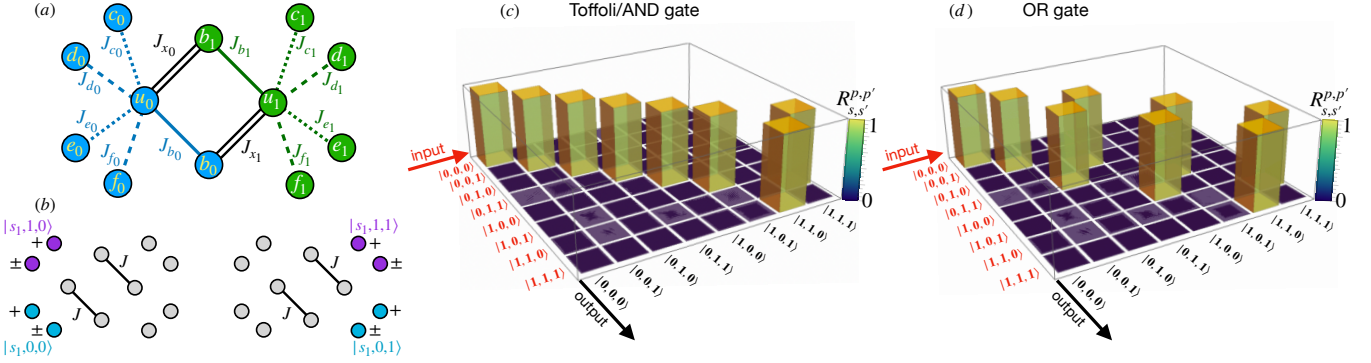


FIG. 4. (a) Schematic of the lattice composed of left (0) and right (1) pentapods respectively colored in blue and green. The two tripods are connected via the hopping J_{x_L} and J_{x_R} . (b) Three qubits encoding states $|b(s_1, s_2, p)\rangle$ with two control qubits $s_1, s_2 = \pm$ and a target $p = 0, 1$ qubits. At the initial parameters $J_{\ell_p} = 0$ for $\ell = c, d, e, f, x$ and $J_{b_p} = J$ for $p = L, R$ of the driving cycle, the states correspond to the eight zero-energy degenerate eigenstates. (c) Quantum state tomography for the Toffoli gate. The driving cycle is shown in the top-right corner. (d) Same as (c) for a quantum version of the OR gate.

with a star topology, where M ones are connected to a central guide u , and it has $M - 1$ zero-energy states [44, 45, 67]. The Hamiltonians of the p -th M -pod is

$$H_p^{(M)} = \sum_{\ell \in [1, M]} J_{\ell, p} (a_{\ell, p}^\dagger a_{\ell, p} + \text{H.c.}) \quad p = 0, 1 \quad (6)$$

with $J_{\ell, p}$ denoting the coupling strengths of the ℓ -th peripheral waveguide $a_{\ell, p}$ to the central central one u_p . For $M = 2^m + 1$, each M -pod has 2^m zero-energy states which can be used to encode m qubit.

The array with two coupled M -pods has the following Hamiltonian

$$H^{(M)} = H_0^{(M)} + H_1^{(M)} + H_X \quad (7)$$

where the coupling Hamiltonian between the M -pods is $H_X = (J_{x_0} a_{1,1}^\dagger u_0 + J_{x_1} a_{1,0}^\dagger u_1 + \text{H.c.})$. The $2 \cdot 2^m$ zero-energy states of the Hamiltonian $H^{(M)}$ yield the encoding of m control qubits and one target qubit [68].

Let us unfold this extension on the *Toffoli* gate. This gate is a doubly-controlled NOT – *i.e.* it applies a NOT gate conditioned on $m = 2$ control qubits, namely $\text{CCNOT} = |0\rangle\langle 0| \otimes \text{I}_4 + |1\rangle\langle 1| \otimes \text{CNOT}$, which is an important component in quantum search algorithms [69–71]. We realize the Toffoli gate by replacing each tripod in Fig. 1(b) with 5-pods, as shown in Fig. 4(a). The Hamiltonian of each 5-pods $H_p^{(5)}$, which we dub *pentapods*, is $H_p = (J_{b_p} b_p^\dagger + J_{c_p} c_p^\dagger + J_{d_p} d_p^\dagger + J_{e_p} e_p^\dagger + J_{f_p} f_p^\dagger) u_p + \text{H.c.}$. The spectrum of the resulting array in Fig. 4(a) consists of eight degenerate modes $\{|\psi_j\rangle\}_{j=1}^8$ at energy $E_0 = 0$ and four non-degenerate modes, see appendix A and Ref [67] for more details.

For $J_{b_0} = J_{b_1} = J$ and all other couplings vanishing, the orthonormal zero modes are supported exclusively on to the disconnected external sites of the two pentapods, namely, they are linear combinations of the states $|c_0\rangle, |d_0\rangle, |e_0\rangle$ and $|f_0\rangle$ and $|c_1\rangle, |d_1\rangle, |e_1\rangle$ and $|f_1\rangle$. Choos-

ing this initial configuration, limiting ourselves to single-excitation space, we can encode three qubits as follows

$$|s_1, s_2, p\rangle = \frac{s_2}{\sqrt{2}} (|c_p\rangle + (2s_1 - 1)|d_p\rangle) + \frac{1 - s_2}{\sqrt{2}} (|e_p\rangle + (2s_1 - 1)|f_p\rangle) \quad (8)$$

where the *control* qubits are identified by the quantum numbers s_1 and s_2 while the *target* qubit is identified by p . The waveguides b_0 and b_1 are instead used only to couple the two pentapods.

By modulating the hopping terms J_{b_p} , J_{c_p} , and J_{x_p} according to the driving cycle shown in Fig. 3(b), while setting all other couplings to zero ($J_{\ell_p} = 0$ for $\ell = e, f$ and $p = 0, 1$), a Toffoli gate is implemented. The corresponding quantum state tomography R for this gate is shown in Fig. 4(c). This gate is particularly notable because it realizes a reversible AND operation [72]. During the implementation of the Toffoli gate, the waveguides e and f remain decoupled from the rest of the circuit; however, they are activated to implement more complex logical operations.

As an example, Fig. 4(d) shows the quantum state tomography of a reversible OR gate [72]. This gate is obtained by composing three driving cycles of the form shown in Fig. 3(b), each time setting a different group of hopping amplitudes to zero. Specifically, the OR gate is implemented by applying the cycle in Fig. 3(b) three times with the following configurations:

- (i) modulating J_{b_p} , J_{c_p} , and J_{x_p} for $p = 0, 1$, while zeroing all other couplings;
- (ii) modulating J_{b_0} , J_{c_0} , and J_{x_0} on the $p = 0$ tripod and J_{e_1} , J_{f_1} , and J_{x_1} on the $p = 1$ tripod, while zeroing the others;
- (iii) modulating J_{e_0} , J_{f_0} , and J_{x_0} on the $p = 0$ tripod and J_{b_1} , J_{c_1} , and J_{x_1} on the $p = 1$ tripod, while zeroing the others.

These two gates shown in Fig. 4(c,d) are conditional gates

of the form

$$C = \sum_{s_1, s_2} |s_1, s_2\rangle\langle s_1, s_2| \otimes V^{s_1, s_2} \quad (9)$$

where V^{s_1, s_2} is a 2×2 unitary transformation which depend on s_1 and s_2 – hence, extending the conditional gate C_η in Eq. (5) from a single to a doubly controlled gate. The unitaries V^{s_1, s_2} can be implemented by either composing driving cycles that selectively involve a few waveguides only, as in our examples above, or driving cycles that involve all guides simultaneously.

V. IMPLEMENTATION OF A QUERY PROBLEM

We now show that the array in Fig. 1(b), together with the driving cycle in Fig. 2 and 3, can be used to implement quantum computing gate-models. A quantum gate-model consists of (i) a set of qubits, (ii) a sequence of quantum gates acting on them, and (iii) measurements performed on selected qubits.

A specific class of gate models is that of query models, which involve an oracle U_f that encodes an unknown black-box function f to be investigated. Deutsch's algorithm is a paradigmatic example of this class [60]. It determines whether a single-bit Boolean function $f : \{0, 1\} \rightarrow \{0, 1\}$ is constant, $f(0) = f(1)$, or balanced, $f(0) \neq f(1)$, using a single oracle query, whereas any classical strategy requires two. The four possible Boolean functions are summarized in Table I, with f_1 and f_4 constant and f_2 and f_3 balanced.

s	$f_1(s)$	$f_2(s)$	$f_3(s)$	$f_4(s)$
0	0	0	1	1
1	0	1	0	1

TABLE I. Table of the four Boolean functions.

As presented in Ref. [60], the oracle U_f which implement the four Boolean functions is an operator acting on the two qubit states $|s, p\rangle$ defined as $U_f(|s, p\rangle) = |s, p \oplus f(s)\rangle$ where \oplus is the XOR operation (i.e. the sum Modulo 2). The query of the Deutsch's algorithm, as schematically recapped in Fig. 5(a), consists in considering a superposition state $|+, -\rangle$ obtained by applying the Hadamard gates on both control and target qubits on an initial input $|0, 1\rangle$, as explicitly detailed in Appendix D. The oracle U_f discerns the functions in the two classes as

$$U_f(|+, -\rangle) = \begin{cases} (-1)^{f(0)}|+, -\rangle & \text{constant} \\ (-1)^{f(0)}|-, -\rangle & \text{balanced} \end{cases} \quad (10)$$

The four operators U_f can be obtained via four different combinations of the CNOT gate and single qubit NOT gate [60]. In our photonic array Fig. 1(b), these four oracle operators are implemented through proper combination of the driving cycles in Fig. 2(a,b) and

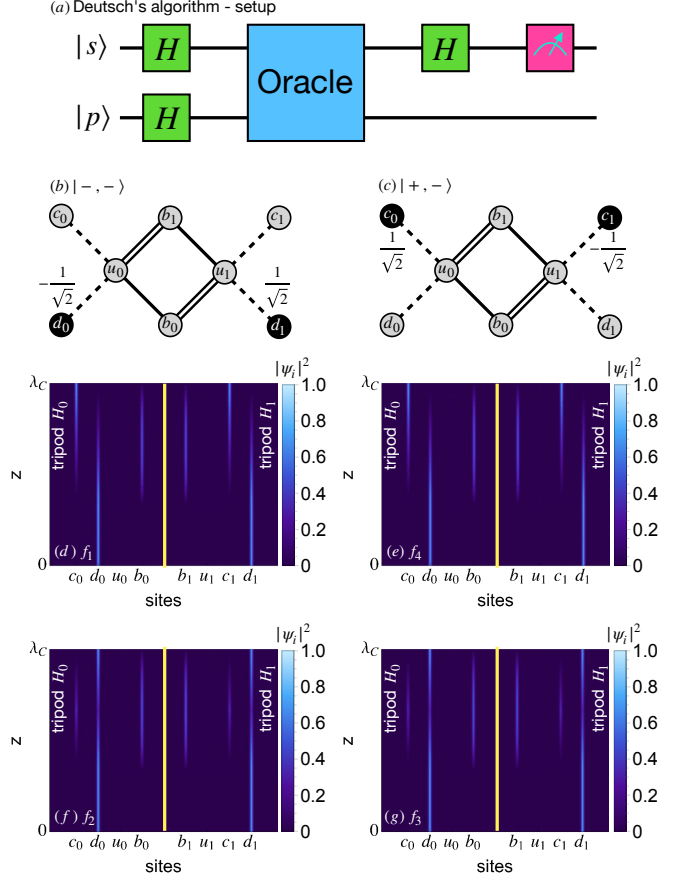


FIG. 5. (a) Illustration of the Deutsch's algorithm. (b,c) Superposition states $|+, -\rangle$ and $|-, -\rangle$. (d,e) Propagation of $|-, -\rangle$ over one cycle period for $\alpha_0 = \pm 1$ and $\alpha_1 = \pm 1$ which respectively implement the constant functions f_1 and f_4 . (f,g) Same as (d,e) for $\alpha_0 = \pm 1$ and $\alpha_1 = \mp 1$ which respectively implement the balanced functions f_2 and f_3 . The yellow lines separate the 0 and the 1 tripods.

Fig. 3(b). However, an alternative and less cumbersome way to implement the oracles comes from exploiting the symmetries of the array Fig. 1(b). Let us impose $J_{d_p} = \alpha_p J_{c_p}$ for $\alpha_p = \pm 1$ in each tripod that – i.e. $H_p = (J_{b_p} b_p^\dagger + J_{c_p} c_p^\dagger + \alpha_p J_{c_p} d_p^\dagger) u_p + \text{H.c.}$ for $p = 0, 1$. Consequently, the driving cycle in Fig. 3(b) yields four holonomies W_{α_0, α_1} – among which the holonomy corresponding to the CNOT can be obtained for $\alpha_0 = 1$ and $\alpha_1 = 1$ and the holonomy corresponding to the SWAP can be obtained for $\alpha_0 = 1$ and $\alpha_1 = -1$. In our photonic array in Fig. 1(b), the superposition states read $|-, -\rangle = \frac{1}{\sqrt{2}}(-|d_0\rangle + |d_1\rangle)$ and $|+, -\rangle = \frac{1}{\sqrt{2}}(|c_0\rangle - |c_1\rangle)$ – respectively shown in Fig. 5(b,c). In Fig. 5(d-g) we show the single queries which distinguish the identity functions f_1, f_4 (shown in Fig. 5(d,e)) from the balanced functions f_2, f_3 (shown in Fig. 5(f,g)).

Let us conclude by conjecturing that the proposed extension of the array from interconnected tripods to interconnected M -pods may pave the way to generalize this

procedure. Indeed, setting $M = 2^m + 1$ could allow the photonic implementation of the Deutsch-Jozsa quantum algorithm via non-Abelian holonomies. This is an algorithm that efficiently distinguish m -bits binary functions $f(s) : \{0, 1\}^m \rightarrow \{0, 1\}$ between constant (the function returns the same value for all 2^m inputs) and balanced (the function returns 0 for half 2^{m-1} inputs and 1 for the remaining half).

VI. CONCLUSIONS

Recent work on non-Abelian Thouless pumping [4, 13, 16], non-Abelian braiding [5, 12, 73, 74], and quantum walks [20] has demonstrated that holonomies in photonic waveguide arrays can be used to control light propagation, enabling the engineering of topological effects.

In the present work, we explore the possibility of encoding the state of single and multiple qubits in the position of a single photon within a waveguide array, and we investigate how non-Abelian holonomies can be used to implement different quantum gates realizing an holonomic version of linear optic quantum computing protocols [48]. Our control strategy is based on the paradigm of *adiabatic population transfer*, similar to that employed in STIRAP atomic protocols. Accordingly, we focus on lattices with the structure of single or coupled M-pods, or star graphs, where a single site is coupled to M peripheral sites. Within these structures, we show that it is possible to engineer manipulations in which the structure of the single-photon wavefunction on a single M -pod with $M = 2^m + 1$ acts as m control qubits, while the placement on one or another M-pods serves as the target. Within this conceptual framework, we discuss the implementation of (i) Single-qubit gates, such as the Hadamard and phase gates, and (ii) Multi-qubit gates, including the CNOT and other multi-controlled gates.

We further show that the proposed photonic array can realize notable quantum query algorithms, such as the Deutsch algorithm, where the adiabatic evolution operator associated with a holonomy acts as the oracle. This holonomic implementation of quantum query problems reframes both the oracle and queries in terms of geometric holonomies. Our approach thus opens a novel direction for leveraging non-Abelian holonomies in quantum algorithms and quantum computing.

ACKNOWLEDGEMENT

This work was co-funded by Project PNRR MUR PE 0000023-NQSTI, Project PNRR MUR project CN 00000013-ICSC, Fondazione Cariplo grant 2023-2594, and the European Union (HORIZON-ERC-2023-ADG HYPERSPIM project Grant No. 101139828). Views and opinions expressed are however those of the author(s) only and do not necessarily reflect those of the European Union of the European Research Council. Neither the

European Union nor the granting authority can be held responsible for them.

DATA AVAILABILITY

The data that support the findings of this article are not publicly available. The data are available from the authors upon reasonable request.

Appendix A: Eight-sites array and holonomies

The Hamiltonian of the photonic array written explicitly reads

$$\begin{aligned} H &= H_0 + H_1 + H_T \\ &= (J_{b_0} b_0^\dagger + J_{c_0} c_0^\dagger + J_{d_0} d_0^\dagger) u_0 \\ &\quad + (J_{b_1} b_1^\dagger + J_{c_1} c_1^\dagger + J_{d_1} d_1^\dagger) u_1 \\ &\quad + J_{x_0} b_1^\dagger u_0 + J_{x_1} b_0^\dagger u_1 + \text{H.c.} \end{aligned} \quad (\text{A1})$$

which has matrix

$$H = \begin{pmatrix} 0 & J_{b_0} & J_{c_0} & J_{d_0} & 0 & J_{x_0} & 0 & 0 \\ J_{b_0} & 0 & 0 & 0 & J_{x_1} & 0 & 0 & 0 \\ J_{c_0} & 0 & 0 & 0 & 0 & 0 & 0 & 0 \\ J_{d_0} & 0 & 0 & 0 & 0 & 0 & 0 & 0 \\ 0 & J_{x_1} & 0 & 0 & 0 & J_{b_1} & J_{c_1} & J_{d_1} \\ J_{x_0} & 0 & 0 & 0 & J_{b_1} & 0 & 0 & 0 \\ 0 & 0 & 0 & 0 & J_{c_1} & 0 & 0 & 0 \\ 0 & 0 & 0 & 0 & J_{d_1} & 0 & 0 & 0 \end{pmatrix} \quad (\text{A2})$$

Due to chiral symmetry, this array has four degenerate eigenenergies at $E_0 = 0$ for any value of the parameters. The other four non-degenerate eigenenergies are

$$\begin{aligned} E &= \\ &\pm \frac{1}{\sqrt{2}} \left\{ J_{b_0}^2 + J_{b_1}^2 + J_{c_0}^2 + J_{c_1}^2 + J_{d_0}^2 + J_{d_1}^2 + J_{x_0}^2 + J_{x_1}^2 \right. \\ &\pm \left[(J_{b_0}^2 + J_{b_1}^2 + J_{c_0}^2 + J_{c_1}^2 + J_{d_0}^2 + J_{d_1}^2 + J_{x_0}^2 + J_{x_1}^2)^2 \right. \\ &+ 4 \left(2J_{b_0} J_{b_1} J_{x_0} J_{x_1} - (J_{c_0}^2 + J_{d_0}^2 + J_{x_0}^2)(J_{c_1}^2 + J_{d_1}^2 + J_{x_1}^2) \right. \\ &\left. \left. - J_{b_1}^2 (J_{c_0}^2 + J_{d_0}^2) - J_{b_0}^2 (J_{b_1}^2 + J_{c_1}^2 + J_{d_1}^2) \right) \right\}^{\frac{1}{2}} \end{aligned} \quad (\text{A3})$$

Chirality constrains the four eigenstates onto the majority subarray $\mathcal{M} = \{b_0, c_0, d_0, b_1, c_1, d_1\}$. Degeneracy implies that there exist arbitrary choices of orthonormal basis $\mathcal{B} = \{|\psi_1\rangle, \dots, |\psi_4\rangle\}$ of the $E_0 = 0$ degenerate subspace. In the following computation of the Wilczek-Zee connection

$$[\Gamma_z]_{\nu\nu'} = \langle \psi_\nu | i\partial_z | \psi_{\nu'} \rangle \quad (\text{A4})$$

used to obtain the holonomy

$$W(z_0, z_1) = e^{i\theta_d} P \exp \left[i \int_{z_0}^{z_1} \Gamma_z dz \right] \quad (\text{A5})$$

we specify basis \mathcal{B} used to compute Γ_z for each gate. This does not affect the calculation nor loose generality, but avoid us to report four cumbersome eigenstates.

Appendix B: Single qubit gates

To implement single qubit Pauli gates represented by σ_y ad σ_z , we set $J_{x_0} = J_{x_1} \equiv 0$ for all $z \in \mathbb{R}$. In this set-up, the four non-zero modes in Eq. (A3) reduce to $E = \left\{ \pm \sqrt{J_{c_0}^2 + J_{d_0}^2 + J_{b_0}^2}, \pm \sqrt{J_{c_1}^2 + J_{d_1}^2 + J_{b_1}^2} \right\}$. An orthonormal basis of zero-modes for this specific configuration is:

$$\begin{aligned} |\psi_1^y(z)\rangle &= \frac{J_{d_0}|c_0\rangle - J_{c_0}|d_0\rangle}{\delta_0} & (B1) \\ |\psi_2^y(z)\rangle &= \frac{J_{d_1}|c_1\rangle - J_{c_1}|d_1\rangle}{\delta_1} \\ |\psi_3^y(z)\rangle &= \frac{J_{b_0}(J_{c_0}|c_0\rangle + J_{d_0}|d_0\rangle) - \delta_0^2|b_0\rangle}{\delta_0\Delta_0} \\ |\psi_4^y(z)\rangle &= \frac{J_{b_1}(J_{c_1}|c_1\rangle + J_{d_1}|d_1\rangle) - \delta_1^2|b_1\rangle}{\delta_1\Delta_1} \end{aligned}$$

where $\delta_p = \sqrt{J_{c_p}^2 + J_{d_p}^2}$ and $\Delta_p = \sqrt{J_{c_p}^2 + J_{d_p}^2 + J_{b_p}^2}$ for $p = 0, 1$. At the starting point of the evolution where the parameters are $J_{c_p} = J_{d_p} = 0, J_{b_p} = J$, these eigenstates reduce to the encoding states $|s, p\rangle$ for $p = 0, 1$ and $s = 0, 1$ as in Eq. (C5). Let us compute the auxiliary terms $A_{\nu\nu'}$ useful to obtain the connection Γ_z in Eq. (C5), here written as

$$\begin{aligned} A_{\nu\nu'} &= i \left\{ \langle \psi_\nu | \partial_{J_{c_0}} | \psi_{\nu'} \rangle, \langle \psi_\nu | \partial_{J_{d_0}} | \psi_{\nu'} \rangle, \langle \psi_\nu | \partial_{J_{b_0}} | \psi_{\nu'} \rangle, \right. \\ &\quad \left. \langle \psi_\nu | \partial_{J_{c_1}} | \psi_{\nu'} \rangle, \langle \psi_\nu | \partial_{J_{d_1}} | \psi_{\nu'} \rangle, \langle \psi_\nu | \partial_{J_{b_1}} | \psi_{\nu'} \rangle \right\} \end{aligned} \quad (B2)$$

The only relevant terms are A_{13} and A_{24} , which read:

$$\begin{aligned} A_{13} &= \frac{iJ_{b_0}}{\delta_0^2\Delta_0} \{J_{c_0}, -J_{d_0}, 0, 0, 0, 0\} & (B3) \\ A_{24} &= \frac{iJ_{b_1}}{\delta_1^2\Delta_1} \{0, 0, 0, J_{c_1}, -J_{d_1}, 0\} \end{aligned}$$

with $A_{31} = -A_{13}$ and $A_{42} = -A_{24}$. The Wilczek-Zee connection then reads

$$\begin{aligned} \Gamma_z &= \frac{J_{b_0}(J_{d_0}\dot{J}_{c_0} - J_{c_0}\dot{J}_{d_0})}{\delta_0^2\Delta_0} \sigma_y \otimes \frac{\sigma_0 + \sigma_z}{2} \\ &\quad + \frac{J_{b_1}(J_{d_1}\dot{J}_{c_1} - J_{c_1}\dot{J}_{d_1})}{\delta_1^2\Delta_1} \sigma_y \otimes \frac{\sigma_0 - \sigma_z}{2} \end{aligned} \quad (B4)$$

For closed paths γ_p in the parameter space, the path integrals yield $\xi_0 = \oint_{\gamma_0} [\Gamma_z]_{13} d\gamma$ and $\xi_1 = \oint_{\gamma_1} [\Gamma_z]_{24} d\gamma$. In Eq. (A5), this results in:

$$\begin{aligned} W(\gamma) &= \begin{pmatrix} \cos \xi_0 & 0 & \sin \xi_0 & 0 \\ 0 & \cos \xi_1 & 0 & \sin \xi_1 \\ -\sin \xi_0 & 0 & \cos \xi_0 & 0 \\ 0 & -\sin \xi_1 & 0 & \cos \xi_1 \end{pmatrix} \\ &= [\cos \xi_0 \sigma_0 + i \sin \xi_0 \sigma_y] \otimes \frac{\sigma_0 + \sigma_z}{2} \\ &\quad + [\cos \xi_1 \sigma_0 + i \sin \xi_1 \sigma_y] \otimes \frac{\sigma_0 - \sigma_z}{2} \end{aligned} \quad (B5)$$

These are two independent σ_y rotations for single qubits in each tripod. Loops of the kind shown in Fig. 6, split in three separate branches ℓ_1 , ℓ_2 and ℓ_3 respectively colored in red, blue and green, allow to implement, among the others, the Hadamard and the NOT gates.

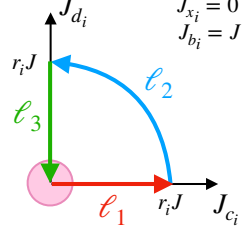


FIG. 6. Driving cycle γ_{σ_y} split in three branches ℓ_1 (red), ℓ_2 (blue) and ℓ_3 (green).

The first and third branches ℓ_1 and ℓ_3 yield zeros in Eq. (B4) as along them J_{c_p} and J_{d_p} are respectively zero. Along ℓ_2 , $J_{b_p} = J$ while $J_{c_p} = r_p J \cos \theta$ and $J_{d_p} = r_p J \sin \theta$ for $\theta \in [0, \frac{\pi}{2}]$. The prefactors of the Pauli matrix tensor products in Eq. (B4) then reduce to $\frac{1}{\sqrt{r_p^2+1}}$. Hence, in Eq. (B5) the angles are $\eta_p = \frac{\pi}{2\sqrt{r_p^2+1}}$. The Hadamard gate is achieved by choosing $r_p = \sqrt{3}$, which implies $\eta_p = \frac{\pi}{4}$. A NOT gate obtained for $\eta_p = \frac{\pi}{2}$ in Eq. (B5) can be achieved by either extending the quarter circle to a half circle (*i.e.* for $\theta \in [0, \pi]$) or by simply repeating the loop γ_{σ_y} in Fig. 6 twice. The holonomy in Eq. (B5) for $\xi_0 = \frac{\pi}{4}$ and $\xi_1 = \frac{\pi}{2}$ hence reduces to

$$\begin{aligned} W &= \frac{1}{\sqrt{2}} \begin{pmatrix} 1 & 0 & 1 & 0 \\ 0 & 0 & 0 & \sqrt{2} \\ -1 & 0 & 1 & 0 \\ 0 & -\sqrt{2} & 0 & 0 \end{pmatrix} \\ &= \frac{\sigma_0 + i\sigma_y}{\sqrt{2}} \otimes \frac{\sigma_0 + \sigma_z}{2} + i\sigma_y \otimes \frac{\sigma_0 - \sigma_z}{2} \end{aligned} \quad (B6)$$

In Fig. 7, we show the evolution of the states $|1, 0\rangle$ [panel(a)] and $|0, 0\rangle$ [panel(b)] in the tripod H_0 via the cycle in Fig. 6 defined for $\xi_0 = \frac{\pi}{4}$. The two tripods are disjoint as the connecting Hamiltonian $H_T = 0$. Both panels show that for $\xi_0 = \frac{\pi}{4}$, the initial states end respectively in a superposition $\frac{|1,0\rangle - |0,0\rangle}{\sqrt{2}}$ and $\frac{|1,0\rangle + |0,0\rangle}{\sqrt{2}}$, which correspond to a $\frac{\pi}{4}$ rotation.

To perform a phase qubit σ_z , we assume $J_{c_p} = J_{d_p}$ in both tripods $p = 0, 1$ and turn the hoppings J_{b_p} complex, *i.e.* $J_{b_p} = J_{b_{i,1}} + e^{i\phi_p} J_{b_{i,2}}$ for phases ϕ_p . An orthonormal basis of zero-modes, for this specific configuration, reads:

$$\begin{aligned} |\psi_1^z(z)\rangle &= \frac{|c_0\rangle - |d_0\rangle}{\sqrt{2}} & (B7) \\ |\psi_2^z(z)\rangle &= \frac{|c_1\rangle - |d_1\rangle}{\sqrt{2}} \\ |\psi_3^z(z)\rangle &= \frac{J_{b_0}(|c_0\rangle + |d_0\rangle) - J_{c_0}|b_1\rangle}{\epsilon_0} \\ |\psi_4^z(z)\rangle &= \frac{J_{b_1}(|c_1\rangle + |d_1\rangle) - J_{c_1}|b_0\rangle}{\epsilon_1} \end{aligned}$$

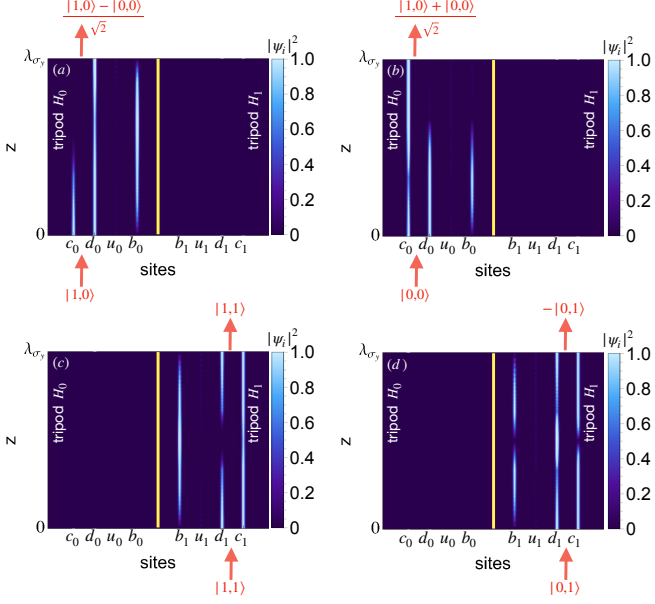


FIG. 7. (a,b) Evolution of the $|1,0\rangle$ and $|0,0\rangle$ respectively via cycle in Fig. 6 with $\xi_0 = \frac{\pi}{4}$ in the tripod H_0 . (c,d) Evolution of the $|1,1\rangle$ and $|0,1\rangle$ respectively via cycle in Fig. 8 in the tripod H_1 . The yellow lines separate the 0 and the 1 tripods.

with $\epsilon_p = \sqrt{2(2J_{c_p}^2 + |J_{b_p}|^2)}$. At the initial point of the cycle where the parameters are $J_{c_p} = 0$, $J_{b_{i,1}} = J$ and $J_{b_{i,2}} = 0$, these eigenstates reduce to the encoding states $|s, p\rangle$ as in Eq. (3). The auxiliary terms $A_{\nu\nu'}$ useful to obtain the connection Γ_z in Eq. (C5), here are:

$$A_{\nu\nu'} = i \left\{ \langle \psi_\nu | \partial_{J_{c_0}} | \psi_{\nu'} \rangle, \langle \psi_\nu | \partial_{J_{b_{0,1}}} | \psi_{\nu'} \rangle, \langle \psi_\nu | \partial_{J_{b_{0,2}}} | \psi_{\nu'} \rangle, \langle \psi_\nu | \partial_{J_{c_1}} | \psi_{\nu'} \rangle, \langle \psi_\nu | \partial_{J_{b_{1,1}}} | \psi_{\nu'} \rangle, \langle \psi_\nu | \partial_{J_{b_{1,2}}} | \psi_{\nu'} \rangle \right\} \quad (B8)$$

The only relevant terms are A_{33} and A_{44} , which read

$$A_{33} = \frac{\sin \phi_0}{\epsilon_0^2} \{0, J_{b_{0,2}}, -J_{b_{0,1}}, 0, 0, 0, 0\} \quad (B9)$$

$$A_{44} = \frac{\sin \phi_1}{\epsilon_1^2} \{0, 0, 0, 0, J_{b_{1,1}}, -J_{b_{1,2}}\}$$

The Wilczek-Zee connection then reads

$$\Gamma_z = \frac{\sin \phi_0 (J_{b_{0,2}} \dot{J}_{b_{0,1}} - J_{b_{0,1}} \dot{J}_{b_{0,2}})}{\epsilon_0^2} \frac{\sigma_0 - \sigma_z}{2} \otimes \frac{\sigma_0 + \sigma_z}{2} + \frac{\sin \phi_1 (J_{b_{1,2}} \dot{J}_{b_{1,1}} - J_{b_{1,1}} \dot{J}_{b_{1,2}})}{\epsilon_1^2} \frac{\sigma_0 - \sigma_z}{2} \otimes \frac{\sigma_0 - \sigma_z}{2} \quad (B10)$$

For a closed path γ in the parameter space, the path integrals yield $\varphi_0 = \oint_{\gamma_0} [\Gamma_z]_{33} d\gamma$ and $\varphi_1 = \oint_{\gamma_1} [\Gamma_z]_{44} d\gamma$.

In Eq. (A5), this results

$$W(z_0, z_1) = \begin{pmatrix} 1 & 0 & 0 & 0 \\ 0 & 1 & 0 & 0 \\ 0 & 0 & e^{i\varphi_0} & 0 \\ 0 & 0 & 0 & e^{i\varphi_1} \end{pmatrix} = \frac{\sigma_0 - \sigma_z}{2} \otimes \left[e^{i\varphi_0} \frac{\sigma_0 + \sigma_z}{2} + e^{i\varphi_1} \frac{\sigma_0 - \sigma_z}{2} \right] + \frac{\sigma_0 + \sigma_z}{2} \otimes \sigma_0 \quad (B11)$$

A typical loop γ_{σ_z} that provides a phase shift gate is shown in Fig. 8, split in three branches ℓ_1 , ℓ_2 and ℓ_3 colored in red, blue and green, respectively. The first and

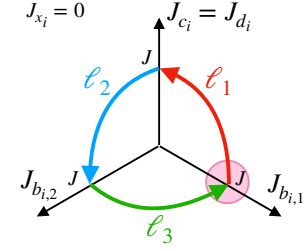


FIG. 8. Driving cycle γ_{σ_z} split in three branches ℓ_1 (red), ℓ_2 (blue) and ℓ_3 (green).

the third branches ℓ_1 and ℓ_3 yield zeroes in Eq. (B10) as along them $J_{b_{i,1}}$ and $J_{b_{i,2}}$ are respectively zero. Along ℓ_2 the hopping $J_{c_p} = 0 = J_{d_p}$, which implies that the prefactors of the Pauli matrix tensor products in Eq. (B10) are the derivative in z of the complex parameters – i.e. $\partial_z J_{b_L} = [\Gamma_x]_{33}$ and $\partial_z J_{b_R} = [\Gamma_x]_{44}$. In this branch ℓ_2 , where $J_{b_{i,2}} = J \cos \theta$ and $J_{b_{i,1}} = J \sin \theta$ for $\theta \in [0, \frac{\pi}{2}]$, the path integrals reduces to $\varphi_0 = \oint_{\gamma} [\Gamma_z]_{33} d\gamma = \phi_L$ and $\varphi_1 = \oint_{\gamma} [\Gamma_z]_{44} d\gamma = \phi_R$. Hence, the holonomy in Eq. (B11) represent two relative phase rotation gates, one in each tripod H_L and H_R . These rotations reduce to two σ_z gates, one per tripod, by choosing $\phi_p = \pi$, whose matrix is

$$W(z_0, z_1) = \begin{pmatrix} 1 & 0 & 0 & 0 \\ 0 & 1 & 0 & 0 \\ 0 & 0 & -1 & 0 \\ 0 & 0 & 0 & -1 \end{pmatrix} = \sigma_z \otimes \sigma_0 \quad (B12)$$

In Fig. 7, we show the evolution of the states $|1,1\rangle$ [panel(c)] and $|0,1\rangle$ [panel(d)] in the tripod H_1 via the cycle in Fig. 8. The two tripods are disjoint as the connecting Hamiltonian $H_T = 0$. These panels show that for $\xi_0 = \frac{\pi}{4}$, the initial state $|1,1\rangle$ is mapped into itself, while $|0,1\rangle$ flips sign.

Appendix C: Two qubits gates

Let us discuss the CNOT and the SWAP gate. To realize the former one, we consider a fully symmetric structure where $J_{x_0} = J_{x_1} \equiv J_x$, $J_{b_0} = J_{b_1} \equiv J_b$ and

$J_{c_0} = J_{c_1} = J_{d_0} = J_{d_1} \equiv J_c$ for which the Hamiltonian reduces to:

$$H(z) = J_b(b_0^\dagger u_0 + b_1^\dagger u_1) + J_x(b_1^\dagger u_0 + b_0^\dagger u_1) + J_c[(c_0^\dagger + d_0^\dagger)u_0 + (c_1^\dagger + d_1^\dagger)u_1] + \text{H.c.} \quad (\text{C1})$$

In this set-up, the four non-zero modes in Eq. (A3) reduce to $E = \pm\sqrt{2J_c^2 + (J_x \pm J_b)^2}$. We introduce an orthonormal basis of zero-modes for this specific driving cycle – hence, we denote the basis with an apex c

$$|\psi_1^c(z)\rangle = \frac{|c_0\rangle - |d_0\rangle}{\sqrt{2}} \quad (\text{C2})$$

$$|\psi_2^c(z)\rangle = \frac{|c_1\rangle - |d_1\rangle}{\sqrt{2}}$$

$$|\psi_3^c(z)\rangle = \frac{J_b(2J_c^2 - J_x^2 + J_b^2)|s_0\rangle + J_x(2J_c^2 + J_x^2 - J_b^2)|s_1\rangle}{R_3} + \frac{\sqrt{2}J_c(J_b^2 + 2J_c^2 + J_x^2)|b_0\rangle - 2\sqrt{2}J_xJ_bJ_c|b_1\rangle}{R_3} \quad (\text{C3})$$

$$|\psi_4^c(z)\rangle = \frac{J_x|s_0\rangle + J_b|s_1\rangle - \sqrt{2}J_c|b_1\rangle}{R_4}$$

where $|s_0\rangle = \frac{|c_0\rangle + |d_0\rangle}{\sqrt{2}}$, $|s_1\rangle = \frac{|c_1\rangle + |d_1\rangle}{\sqrt{2}}$, $N_\pm = \sqrt{2J_c^2 + (J_x \pm J_b)^2}$, $R_4 = \sqrt{2J_c^2 + J_x^2 + J_b^2}$ and $R_3 = R_4N_+N_-$. At the initial parameters considered for any cycle $J_x = J_c = 0$, $J_b = J$, these eigenstates in Eq. (C4) reduce to the two qubits encoding states $|s, p\rangle$ for $p = 0, 1$ and $s = 0, 1$

$$|\psi_1^c(0)\rangle = \frac{|c_0\rangle - |d_0\rangle}{\sqrt{2}} \equiv |0, 0\rangle \quad (\text{C4})$$

$$|\psi_2^c(0)\rangle = \frac{|c_1\rangle - |d_1\rangle}{\sqrt{2}} \equiv |0, 1\rangle$$

$$|\psi_3^c(0)\rangle = \frac{|c_0\rangle + |d_0\rangle}{\sqrt{2}} \equiv |1, 0\rangle$$

$$|\psi_4^c(0)\rangle = \frac{|c_1\rangle + |d_1\rangle}{\sqrt{2}} \equiv |1, 1\rangle$$

We calculate each element of Γ_z in Eq. (A4)

$$[\Gamma_z]_{\nu\nu'} = \mathbf{A}_{\nu\nu'} \cdot \mathbf{V} \quad (\text{C5})$$

where $\mathbf{V} = (\dot{J}_b, \dot{J}_c, \dot{J}_x)$ and $\mathbf{A}_{\nu\nu'}$ are given by

$$A_{\nu\nu'} = i \{ \langle \psi_\nu | \partial_{J_b} | \psi_{\nu'} \rangle, \langle \psi_\nu | \partial_{J_c} | \psi_{\nu'} \rangle, \langle \psi_\nu | \partial_{J_x} | \psi_{\nu'} \rangle \} \quad (\text{C6})$$

Since all eigenvectors are real, then $\langle \psi_\nu | \partial_{J_\ell} | \psi_\nu \rangle = 0$ for all each $\nu = 1, \dots, 4$ and for each $\ell = b, c, x$. Hence, the diagonal elements of the connection Γ_z are zero. Furthermore, since $|\psi_1\rangle$ and $|\psi_2\rangle$ and independent on the parameter J_ℓ , the only non-zero terms in Γ_z are those induced by $|\psi_3\rangle$ and $|\psi_4\rangle$. It then follows

$$A_{34} = \frac{i}{R_3^2 N_+ N_-} \{ J_x(J_b^2 - 2J_c^2 - J_x^2), 4J_bJ_cJ_x, J_b(J_x^2 - J_b^2 - 2J_c^2) \} \quad (\text{C7})$$

with $A_{43} = -A_{34}$. The Wilczek-Zee connection then reads

$$\begin{aligned} \Gamma_z = & \frac{2J_xJ_c^2\dot{J}_b - 4J_bJ_cJ_x\dot{J}_c + 2J_bJ_c^2\dot{J}_x}{R_3^2 N_+ N_-} \\ & - \frac{J_bJ_x(J_b\dot{J}_b + J_x\dot{J}_x) + J_x^3\dot{J}_b + J_b^3\dot{J}_x}{R_3^2 N_+ N_-} \frac{\sigma_0 - \sigma_z}{2} \otimes \sigma_y \\ & = f_{\text{CN}}(J_c, J_b, J_x)(\sigma_0 - \sigma_z) \otimes \sigma_y \end{aligned} \quad (\text{C8})$$

for the Pauli matrices σ_p with $i = x, y, z$ and the identity σ_0 . For a closed path γ in the parameter space $\{J_b, J_c, J_x\}$, let us define the result of the path integral yields $\eta = \oint_\gamma [\Gamma_z]_{34} d\gamma$. In Eq. (A5), this results

$$\begin{aligned} W(z_0, z_1) = & \frac{\sigma_0 - \sigma_z}{2} \otimes [\cos \eta \sigma_0 + i \sin \eta \sigma_y] + \frac{\sigma_0 + \sigma_z}{2} \otimes \sigma_0 \\ = & \begin{pmatrix} 1 & 0 & 0 & 0 \\ 0 & 1 & 0 & 0 \\ 0 & 0 & \cos \eta & \sin \eta \\ 0 & 0 & -\sin \eta & \cos \eta \end{pmatrix} \end{aligned} \quad (\text{C9})$$

Let us consider the driving cycle γ_C for the CNOT, and split it in three separate branches ℓ_1 , ℓ_2 and ℓ_3 respectively colored in red, blue and green. In each branch ℓ_1 ,

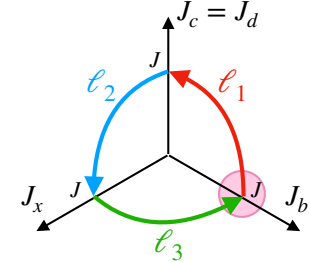


FIG. 9. Driving cycle γ_C split in three branches ℓ_1 (red), ℓ_2 (blue) and ℓ_3 (green).

ℓ_2 and ℓ_3 , only pairs of parameters evolve while the third is set to zero. This immediately sets the first three terms in Eq. (C8) irrelevant as they require the simultaneous variations of all three parameters. The four remaining terms require the simultaneous variation of J_b and J_x – hence, the branches ℓ_1 and ℓ_2 immediately yield zero. Branch ℓ_3 instead reads set $J_b = \cos \theta$ and $J_x = \sin \theta$, with $J_c \equiv 0$. From Eq. (C8)

$$\begin{aligned} [\Gamma_z]_{34} = & \frac{J_x^3\dot{J}_b + J_b^3\dot{J}_x - J_bJ_x(J_b\dot{J}_b + J_x\dot{J}_x)}{(J_x^2 + J_b^2)(J_x^2 - J_b^2)} \\ = & \frac{\cos^4 \theta - \sin^4 \theta}{\sin^2 \theta - \cos^2 \theta} = 1 \end{aligned} \quad (\text{C10})$$

Integrated from 0 to $\frac{\pi}{2}$, it follows that $\eta = \int_0^{\frac{\pi}{2}} [\Gamma_z]_{34} dz = \frac{\pi}{2}$ which, via Eq. (C9) implies that the holonomy W is

$$W_{\text{CN}} = \begin{pmatrix} 1 & 0 & 0 & 0 \\ 0 & 1 & 0 & 0 \\ 0 & 0 & 0 & 1 \\ 0 & 0 & -1 & 0 \end{pmatrix} \quad (\text{C11})$$

$$= \frac{1}{2}[(\sigma_0 + \sigma_z) \otimes \sigma_0 + i(\sigma_0 - \sigma_z) \otimes \sigma_y]$$

For the SWAP, we keep the symmetry conditions $J_{x_L} = J_{x_R} \equiv J_x$, $J_{b_L} = J_{b_R} \equiv J_b$ and $J_{c_L} = J_{d_L} \equiv J_c$ set for the CNOT, and impose an anti-symmetry condition $J_{c_R} = -J_{d_R} \equiv J_c$. The orthonormal basis of zero-modes for this specific driving cycle – hence, we denote the basis with an apex s

$$|\psi_1^s(z)\rangle = \frac{|c_0\rangle - |d_0\rangle}{\sqrt{2}} \quad (\text{C12})$$

$$|\psi_2^s(z)\rangle = \frac{J_x|s_0\rangle + J_b|a_1\rangle - \sqrt{2}J_c|b_1\rangle}{R_3}$$

$$|\psi_3^s(z)\rangle = \frac{J_b(2J_c^2 - J_x^2 + J_b^2)|s_0\rangle + J_x(2J_c^2 + J_x^2 - J_b^2)|a_1\rangle}{R_4} + \frac{\sqrt{2}J_c(J_b^2 + 2J_c^2 + J_x^2)|b_0\rangle - 2\sqrt{2}J_xJ_bJ_c|b_1\rangle}{R_3} \quad (\text{C13})$$

$$|\psi_4^s(z)\rangle = \frac{|c_1\rangle + |d_1\rangle}{\sqrt{2}}$$

where $|a_1\rangle = \frac{|c_1\rangle - |d_1\rangle}{\sqrt{2}}$. Alike for the CNOT, at $J_x = J_c = 0, J_b = J$ these eigenstates in Eq. (C14) reduce to the two qubits encoding states $|s, p\rangle$ for $p = 0, 1$ and $s = 0, 1$ as in Eq. (C5). For the same driving cycle in Fig. 9, the holonomy results in

$$W_{\text{SW}} = \begin{pmatrix} 1 & 0 & 0 & 0 \\ 0 & 0 & 1 & 0 \\ 0 & -1 & 0 & 0 \\ 0 & 0 & 0 & 1 \end{pmatrix} \quad (\text{C14})$$

$$= \frac{1}{2}(\sigma_0 \otimes \sigma_0 - i\sigma_x \otimes \sigma_y + i\sigma_y \otimes \sigma_x + \sigma_z \otimes \sigma_z)$$

Let us obtain the SWAP from the CNOT. An holonomic NOT gate acting on the control qubit on the right tripod H_R can be obtained in Eq. (B5) by setting $\eta_L = 0$ and $\eta_R \frac{\pi}{2}$. These two angles are obtained by (i) in the left tripod H_L keep all the hopping to zero $J_{\ell_L} = 0$ for $\ell = c, d, b$, while (ii) running twice the driving cycle in Fig. (6) in the right tripod H_R . Eq. (B5) then reduces to

$$W_{\text{nR}} = \begin{pmatrix} 1 & 0 & 0 & 0 \\ 0 & 0 & 0 & 1 \\ 0 & 0 & 1 & 0 \\ 0 & -1 & 0 & 0 \end{pmatrix} \quad (\text{C15})$$

$$= \sigma_0 \otimes \frac{\sigma_0 + \sigma_z}{2} + i\sigma_y \otimes \frac{\sigma_0 - \sigma_z}{2}$$

The product

$$W_{\text{nR}}^\dagger W_{\text{CN}} W_{\text{nR}} = \begin{pmatrix} 1 & 0 & 0 & 0 \\ 0 & 0 & 1 & 0 \\ 0 & -1 & 0 & 0 \\ 0 & 0 & 0 & 1 \end{pmatrix} = W_{\text{SW}} \quad (\text{C16})$$

corresponds to the holonomy W_{SW} of the SWAP gate in Eq. (C14).

Appendix D: Deutsch's algorithm

The Deustch's algorithm leverages on quantum superposition to distinguish binary functions f in Table I between constant and balanced with a single measurement. Formally, for a binary function f and a state $|s, p\rangle$ with control qubit s and target qubit p , the oracle U_f of the Deustch's algorithm acts as $U_f(|s, p\rangle) = |s, p \oplus f(s)\rangle$ the XOR $a \oplus b = [a + b]_2$ (sum modulo 2).

Applied on a superposition

$$|s, -\rangle = \frac{1}{\sqrt{2}}(|s, 0\rangle - |s, 1\rangle) \quad (\text{D1})$$

the oracle U_f yields the *phase kickback* property $U_f|s, -\rangle = (-1)^{f(s)}|s, -\rangle$. For a superposition state

$$|+, -\rangle = \frac{1}{\sqrt{2}}(|0, -\rangle + |1, -\rangle) = \frac{1}{2}(|0, 0\rangle - |0, 1\rangle + |1, 0\rangle - |1, 1\rangle) \quad (\text{D2})$$

obtained by applying the Hadamard gates on both control and target on an initial input $|0, 1\rangle$, it then follows that

$$U_f|+, -\rangle = |-\rangle \frac{(-1)^{f(0)}|0\rangle + (-1)^{f(1)}|1\rangle}{\sqrt{2}} = |-\rangle (-1)^{f(0)}|0\rangle + (-1)^{f(0) \otimes f(1)}|1\rangle = \frac{(-1)^{f(0)}|+, -\rangle}{\sqrt{2}} \quad (\text{D3})$$

$$= \begin{cases} (-1)^{f(0)}|+, -\rangle & f(0) \otimes f(1) = 0 \\ (-1)^{f(0)}|-, -\rangle & f(0) \otimes f(1) = 1 \end{cases}$$

A final Hadamard gate on the control qubit s allows then to distinguish constant functions from balanced ones.

We now explicitly show that the photonic array proposed in Fig. 1(a) and the driving cycle in Fig. 3(b) with proper signs of the hopping terms implement the oracle identity in Eq. (D3). Consider the Hamiltonian $H = H_0 + H_1 + H_T$, where $H_T = J_{x_0}b_1^\dagger u_0 + J_{x_1}b_0^\dagger u_1 + \text{H.c.}$ and for $p = 0, 1$ we have that $H_p = (J_{b_p}b_p^\dagger + J_{c_p}c_p^\dagger + \alpha_p J_{c_p}d_p^\dagger)u_p + \text{H.c.}$ with $J_{d_p} = \alpha_p J_{c_p}$ for $\alpha_p = \pm 1$. The

driving cycle in Fig. 3(b) yields four holonomies W_{α_0, α_1}

$$\begin{aligned} W_{1,1} &= \frac{1}{2}[(\sigma_0 + \sigma_z) \otimes \sigma_0 + i(\sigma_0 - \sigma_z) \otimes \sigma_y] \\ W_{1,-1} &= \frac{1}{2}[\sigma_0 \otimes \sigma_0 + \sigma_z \otimes \sigma_z + i(\sigma_y \otimes \sigma_x - \sigma_x \otimes \sigma_y)] \\ W_{-1,1} &= \frac{1}{2}[\sigma_0 \otimes \sigma_0 - \sigma_z \otimes \sigma_z + i(\sigma_y \otimes \sigma_x + \sigma_x \otimes \sigma_y)] \\ W_{-1,-1} &= \frac{1}{2}[(\sigma_0 - \sigma_z) \otimes \sigma_0 + i(\sigma_0 + \sigma_z) \otimes \sigma_y] \end{aligned} \quad (D4)$$

Straightening the minus signs in the holonomies via the phase gate, we obtain the four transformations

$$\begin{aligned} V_{f_1} &= \begin{pmatrix} 1 & 0 & 0 & 0 \\ 0 & 1 & 0 & 0 \\ 0 & 0 & 0 & 1 \\ 0 & 0 & 1 & 0 \end{pmatrix} & V_{f_4} &= \begin{pmatrix} 0 & 1 & 0 & 0 \\ 1 & 0 & 0 & 0 \\ 0 & 0 & 1 & 0 \\ 0 & 0 & 0 & 1 \end{pmatrix} \\ V_{f_2} &= \begin{pmatrix} 1 & 0 & 0 & 0 \\ 0 & 0 & 1 & 0 \\ 0 & 1 & 0 & 0 \\ 0 & 0 & 0 & 1 \end{pmatrix} & V_{f_3} &= \begin{pmatrix} 0 & 0 & 0 & 1 \\ 0 & 1 & 0 & 0 \\ 0 & 0 & 1 & 0 \\ 1 & 0 & 0 & 0 \end{pmatrix} \end{aligned} \quad (D5)$$

We define the functions f_1, \dots, f_4 in Table I via the transformations V_{f_1}, \dots, V_{f_4} in Eq. (D5) by firstly setting the input $x \in \{0, 1\}$ in the two-qubits states as

$$\text{input } \mathcal{I} : \begin{cases} x = 0 \mapsto |0, 0\rangle \\ x = 1 \mapsto |1, 1\rangle \end{cases} \quad (D6)$$

Then we compose V_{f_1}, \dots, V_{f_4} with a measurement done via scalar product $P_1 = \langle 1, 0 | + \langle 1, 1 |$

$$f_\ell(x) = |P_1 \circ V_{f_\ell}|x, x\rangle|^2 \quad (D7)$$

Indeed,

$$\begin{aligned} f_1(x) &= \begin{cases} 0 \xrightarrow{\mathcal{I}} |0, 0\rangle \xrightarrow{V_{f_1}} |0, 0\rangle \xrightarrow{P_1} 0 \\ 1 \xrightarrow{\mathcal{I}} |1, 1\rangle \xrightarrow{V_{f_1}} |1, 0\rangle \xrightarrow{P_1} 0 \end{cases} \\ f_2(x) &= \begin{cases} 0 \xrightarrow{\mathcal{I}} |0, 0\rangle \xrightarrow{V_{f_2}} |0, 0\rangle \xrightarrow{P_1} 0 \\ 1 \xrightarrow{\mathcal{I}} |1, 1\rangle \xrightarrow{V_{f_2}} |1, 1\rangle \xrightarrow{P_1} 1 \end{cases} \\ f_3(x) &= \begin{cases} 0 \xrightarrow{\mathcal{I}} |0, 0\rangle \xrightarrow{V_{f_3}} |0, 1\rangle \xrightarrow{P_1} 1 \\ 1 \xrightarrow{\mathcal{I}} |1, 1\rangle \xrightarrow{V_{f_3}} |1, 0\rangle \xrightarrow{P_1} 0 \end{cases} \\ f_4(x) &= \begin{cases} 0 \xrightarrow{\mathcal{I}} |0, 0\rangle \xrightarrow{V_{f_4}} |0, 1\rangle \xrightarrow{P_1} 1 \\ 1 \xrightarrow{\mathcal{I}} |1, 1\rangle \xrightarrow{V_{f_4}} |1, 1\rangle \xrightarrow{P_1} 1 \end{cases} \end{aligned} \quad (D8)$$

The superposition states where we perform the Deustch's algorithm are

$$\begin{aligned} |+, -\rangle &= \frac{1}{2}(|0, 0\rangle - |0, 1\rangle + |1, 0\rangle - |1, 1\rangle) \\ |-, -\rangle &= \frac{1}{2}(|0, 0\rangle - |0, 1\rangle - |1, 0\rangle + |1, 1\rangle) \end{aligned} \quad (D9)$$

Then

$$\begin{aligned} V_{f_1}(|-, -\rangle) &= \frac{1}{2}(|0, 0\rangle - |0, 1\rangle - |1, 1\rangle + |1, 0\rangle) = |+, -\rangle \\ V_{f_2}(|-, -\rangle) &= \frac{1}{2}(|0, 0\rangle - |1, 0\rangle - |0, 1\rangle + |1, 1\rangle) = |-, -\rangle \\ V_{f_3}(|-, -\rangle) &= \frac{1}{2}(|1, 1\rangle - |0, 1\rangle - |1, 0\rangle + |0, 0\rangle) = |-, -\rangle \\ V_{f_4}(|-, -\rangle) &= \frac{1}{2}(|0, 1\rangle - |0, 0\rangle - |1, 0\rangle + |1, 1\rangle) = |+, -\rangle \end{aligned} \quad (D10)$$

[1] F. Wilczek and A. Zee, Appearance of gauge structure in simple dynamical systems, *Phys. Rev. Lett.* **52**, 2111 (1984).

[2] J. Anandan, Non-adiabatic non-abelian geometric phase, *Physics Letters A* **133**, 171 (1988).

[3] M. V. Berry, Quantal phase factors accompanying adiabatic changes, *Proceedings of the Royal Society of London. A. Mathematical and Physical Sciences* **392**, 45 (1984).

[4] Y.-K. Sun, X.-L. Zhang, F. Yu, Z.-N. Tian, Q.-D. Chen, and H.-B. Sun, Non-abelian thouless pumping in photonic waveguides, *Nature Physics* **18**, 1080 (2022).

[5] Y. Chen, Y. Fan, G. Larsson, J. Xiang, A. He, G. Wang, X.-L. Zhang, G. Ma, Q. Zhou, G. Guo, Y. Su, and X. Guo, High-dimensional non-abelian holonomy in integrated photonics, *Nature Communications* **16**, 3650 (2025).

[6] O. You, S. Liang, B. Xie, W. Gao, W. Ye, J. Zhu, and S. Zhang, Observation of non-abelian thouless pump, *Phys. Rev. Lett.* **128**, 244302 (2022).

[7] J. W. Zwanziger, M. Koenig, and A. Pines, Non-abelian effects in a quadrupole system rotating around two axes, *Phys. Rev. A* **42**, 3107 (1990).

[8] R. G. Unanyan, B. W. Shore, and K. Bergmann, Laser-driven population transfer in four-level atoms: Consequences of non-abelian geometrical adiabatic phase factors, *Phys. Rev. A* **59**, 2910 (1999).

[9] S. Sugawa, F. Salces-Carcoba, A. R. Perry, Y. Yue, and I. B. Spielman, Second chern number of a quantum-simulated non-abelian yang monopole, *Science* **360**, 1429 (2018).

[10] A. A. Abdumalikov Jr, J. M. Fink, K. Juliusson, M. Pechal, S. Berger, A. Wallraff, and S. Filipp, Experimental realization of non-abelian non-adiabatic geometric gates, *Nature* **496**, 482 (2013).

[11] S. Murakami, N. Nagosa, and S.-C. Zhang, SU(2) non-abelian holonomy and dissipationless spin current in semiconductors, *Phys. Rev. B* **69**, 235206 (2004).

[12] Y. Chen, R.-Y. Zhang, Z. Xiong, Z. H. Hang, J. Li, J. Q. Shen, and C. Chan, Non-abelian gauge field optics, *Nature communications* **10**, 3125 (2019).

[13] V. Brosco, L. Pilozzi, R. Fazio, and C. Conti, Non-abelian thouless pumping in a photonic lattice, *Phys. Rev. A* **103**, 063518 (2021).

[14] L. Pilozzi and V. Brosco, Thouless pumping of light with a twist, *Nature Physics* **18**, 968 (2022).

[15] L. Taddia, E. Cornfeld, D. Rossini, L. Mazza, E. Sela, and R. Fazio, Topological fractional pumping with alkaline-earth-like atoms in synthetic lattices, *Phys. Rev. Lett.* **118**, 230402 (2017).

[16] C. Danieli, V. Brosco, L. Pilozzi, and R. Citro, Non-abelian thouless pumping in a rice-mele ladder, *AVS Quantum Science* **7**, 022001 (2025).

[17] T. Iadecola, T. Schuster, and C. Chamon, Non-abelian braiding of light, *Phys. Rev. Lett.* **117**, 073901 (2016).

[18] L.-M. Duan, J. I. Cirac, and P. Zoller, Geometric manipulation of trapped ions for quantum computation, *Science* **292**, 1695 (2001).

[19] V. Brosco, R. Fazio, F. W. J. Hekking, and A. Joye, Non-abelian superconducting pumps, *Phys. Rev. Lett.* **100**, 027002 (2008).

[20] C. Danieli, L. Pilozzi, C. Conti, and V. Brosco, Parity breaking in thouless quantum walks, arXiv:2412.02429, under consideration in *Light: Science and Applications* (2024).

[21] P. Zanardi and M. Rasetti, Holonomic quantum computation, *Physics Letters A* **264**, 94 (1999).

[22] J. Zhang, T. H. Kyaw, S. Filipp, L.-C. Kwek, E. Sjöqvist, and D. Tong, Geometric and holonomic quantum computation, *Physics Reports* **1027**, 1 (2023), geometric and holonomic quantum computation.

[23] A. Y. Kitaev, Quantum computations: algorithms and error correction, *Russian Mathematical Surveys* **52**, 1191 (1997).

[24] P. Solinas, P. Zanardi, and N. Zanghì, Robustness of non-abelian holonomic quantum gates against parametric noise, *Phys. Rev. A* **70**, 042316 (2004).

[25] S.-Y. Sun, L.-N. Ji, F.-F. Cui, Z.-Y. Xue, and T. Chen, Suppression of systematic errors in holonomic quantum gates via multipath correction, *Phys. Rev. A* **110**, 062621 (2024).

[26] X. Y. Sun and P. Z. Zhao, Decoherence mitigation for geometric quantum computation, *Phys. Rev. A* **112**, 032403 (2025).

[27] J. A. Jones, V. Vedral, A. Ekert, and G. Castagnoli, Geometric quantum computation using nuclear magnetic resonance, *Nature* **403**, 869 (2000).

[28] J. Pachos and S. Chountasis, Optical holonomic quantum computer, *Phys. Rev. A* **62**, 052318 (2000).

[29] L. Faoro, J. Siewert, and R. Fazio, Non-abelian holonomies, charge pumping, and quantum computation with josephson junctions, *Phys. Rev. Lett.* **90**, 028301 (2003).

[30] K. Nagata, K. Kuramitani, Y. Sekiguchi, and H. Kosaka, Universal holonomic quantum gates over geometric spin qubits with polarised microwaves, *Nature Communications* **9**, 3227 (2018).

[31] S. Bhattacharyya and S. Bhattacharyya, Holonomic control of a three-qubits system in an nv center using a near-term quantum computer, arXiv:2202.08061 (2022).

[32] Y.-S. Chen, J. Gao, and L.-N. Ji, Realization of universal nonadiabatic holonomic quantum gates in trapped ion system (2025), arXiv:2505.02137 [quant-ph].

[33] D. David, *Quantum theory, the Church-Turing principle and the universal quantum computer* (R. Soc. Lond, 1985).

[34] P. Shor, Fault-tolerant quantum computation, in *Proceedings of 37th Conference on Foundations of Computer Science* (1996) pp. 56–65.

[35] D. Gottesman, Theory of fault-tolerant quantum computation, *Phys. Rev. A* **57**, 127 (1998).

[36] P. Boykin, T. Mor, M. Pulver, V. Roychowdhury, and F. Vatan, A new universal and fault-tolerant quantum basis, *Information Processing Letters* **75**, 101 (2000).

[37] A. Paetznick and B. W. Reichardt, Universal fault-tolerant quantum computation with only transversal gates and error correction, *Phys. Rev. Lett.* **111**, 090505 (2013).

[38] T. Yan, B.-J. Liu, K. Xu, C. Song, S. Liu, Z. Zhang, H. Deng, Z. Yan, H. Rong, K. Huang, M.-H. Yung, Y. Chen, and D. Yu, Experimental realization of non-adiabatic shortcut to non-abelian geometric gates, *Phys. Rev. Lett.* **122**, 080501 (2019).

[39] P. Z. Zhao and D. M. Tong, Nonadiabatic holonomic quantum computation based on a commutation relation, *Phys. Rev. A* **108**, 012619 (2023).

[40] V. Neef, J. Pinske, T. A. W. Wolterink, K. Becker, M. Heinrich, S. Scheel, and A. Szameit, Non-adiabatic holonomies for photonic quantum computing, *Optica Quantum* **3**, 93 (2025).

[41] F. Jin, J. Geng, and H. Zhou, Nonadiabatic holonomic quantum gates in a decoherence-insensitive space, *Phys. Rev. A* **111**, 022620 (2025).

[42] W. Song, X. Liu, J. Sun, O. You, S. Wu, C. Chen, S. Zhu, T. Li, and S. Zhang, Shortcuts to adiabatic non-abelian braiding on silicon photonic chips, *Science Advances* **11**, ead7224 (2025).

[43] V. Neef, J. Pinske, F. Klauck, L. Teuber, M. Kremer, M. Ehrhardt, M. Heinrich, S. Scheel, and A. Szameit, Three-dimensional non-abelian quantum holonomy, *Nature Physics* **19**, 30 (2023).

[44] J. Pinske, L. Teuber, and S. Scheel, Highly degenerate photonic waveguide structures for holonomic computation, *Phys. Rev. A* **101**, 062314 (2020).

[45] J. Pinske and S. Scheel, Symmetry-protected non-abelian geometric phases in optical waveguides with nonorthogonal modes, *Phys. Rev. A* **105**, 013507 (2022).

[46] A. Babazadeh, M. Erhard, F. Wang, M. Malik, R. Nouroozi, M. Krenn, and A. Zeilinger, High-dimensional single-photon quantum gates: Concepts and experiments, *Phys. Rev. Lett.* **119**, 180510 (2017).

[47] R. Lapkiewicz, P. Li, C. Schaeff, N. K. Langford, S. Ramelow, M. Wieśniak, and A. Zeilinger, Experimental non-classicality of an indivisible quantum system, *Nature* **474**, 490 (2011).

[48] P. Kok, W. J. Munro, K. Nemoto, T. C. Ralph, J. P. Dowling, and G. J. Milburn, Linear optical quantum computing with photonic qubits, *Rev. Mod. Phys.* **79**, 135 (2007).

[49] A. Y. Vlasov, Clifford algebras and universal sets of quantum gates, *Phys. Rev. A* **63**, 054302 (2001).

[50] J. Tolar, On clifford groups in quantum computing, *Journal of Physics: Conference Series* **1071**, 012022 (2018).

[51] J. Helsen, J. J. Wallman, and S. Wehner, Representations of the multi-qubit clifford group, *Journal of Mathematical Physics* **59**, 072201 (2018).

[52] M. Bataille, Quantum circuits of cnot gates, arXiv:2009.13247 (2020).

[53] C. Monroe, D. M. Meekhof, B. E. King, W. M. Itano, and D. J. Wineland, Demonstration of a fundamental quantum logic gate, *Phys. Rev. Lett.* **75**, 4714 (1995).

[54] A. Barenco, C. H. Bennett, R. Cleve, D. P. DiVincenzo, N. Margolus, P. Shor, T. Sleator, J. A. Smolin, and H. Weinfurter, Elementary gates for quantum computa-

tion, *Phys. Rev. A* **52**, 3457 (1995).

[55] B. P. Lanyon, M. Barbieri, M. P. Almeida, T. Jennewein, T. C. Ralph, K. J. Resch, G. J. Pryde, J. L. O'brien, A. Gilchrist, and A. G. White, Simplifying quantum logic using higher-dimensional hilbert spaces, *Nature Physics* **5**, 134 (2009).

[56] D. Qin, Y. Chen, and Y. Li, Error statistics and scalability of quantum error mitigation formulas, *npj Quantum Information* **9**, 35 (2023).

[57] B. Zindorf and S. Bose, Efficient implementation of multicontrolled quantum gates, *Phys. Rev. Appl.* **24**, 044030 (2025).

[58] D. Aharonov, A simple proof that toffoli and hadamard are quantum universal, *arXiv: quant-ph/0301040* (2003).

[59] D. Deutsch, Quantum computational networks *Proc. R. Soc. A* **425**, 90 (1989).

[60] R. Portugal, Basic quantum algorithms (2025), *arXiv:2201.10574* [quant-ph].

[61] A. Ramachandran, A. Andrianov, and S. Flach, Chiral flat bands: Existence, engineering, and stability, *Phys. Rev. B* **96**, 161104(R) (2017).

[62] R. Keil, C. Poli, M. Heinrich, J. Arkinstall, G. Weihs, H. Schomerus, and A. Szameit, Universal sign control of coupling in tight-binding lattices, *Phys. Rev. Lett.* **116**, 213901 (2016).

[63] M. Kremer, I. Petrides, E. Meyer, M. Heinrich, O. Zilberberg, and A. Szameit, A square-root topological insulator with non-quantized indices realized with photonic aharonov-bohm cages, *Nature communications* **11**, 907 (2020).

[64] Y.-J. Chang, Y.-H. Lu, Y. Wang, X.-Y. Xu, W.-H. Zhou, W.-H. Cui, X.-W. Wang, J. Gao, L.-F. Qiao, and X.-M. Jin, Symmetry-induced error filtering in a photonic lieb lattice, *Phys. Rev. Lett.* **126**, 110501 (2021).

[65] D. Roman-Cortes, M. Mazanov, R. A. Vicencio, and M. A. Gorlach, Observation of invisibility angle and flat band physics in dipolar photonic lattices, *Nano Letters* **25**, 4291 (2025).

[66] R. A. Vicencio, Multi-orbital photonic lattices, *APL Photonics* **10**, 071101 (2025).

[67] J. R. Morris and B. W. Shore, Reduction of degenerate two-level excitation to independent two-state systems, *Phys. Rev. A* **27**, 906 (1983).

[68] For comparison: (i) each tripod used in Fig. 1(b) has $M = 3 = 2^1 + 1$ which result in a single ($m = 1$) control qubit; while (ii) each pentapod used in Fig. 4(a) has $M = 5 = 2^2 + 1$ which result in two ($m = 2$) control qubits.

[69] C. Figgatt, D. Maslov, K. A. Landsman, N. M. Linke, S. Debnath, and C. Monroe, Complete 3-qubit grover search on a programmable quantum computer, *Nature communications* **8**, 1918 (2017).

[70] C. Gidney and M. Ekerå, How to factor 2048 bit RSA integers in 8 hours using 20 million noisy qubits, *Quantum* **5**, 433 (2021).

[71] J. Chu, X. He, Y. Zhou, J. Yuan, L. Zhang, Q. Guo, Y. Hai, Z. Han, C.-K. Hu, W. Huang, H. Jia, D. Jiao, S. Li, Y. Liu, Z. Ni, L. Nie, X. Pan, J. Qiu, W. Wei, W. Nuerbolati, Z. Yang, J. Zhang, Z. Zhang, W. Zou, Y. Chen, X. Deng, X. Deng, L. Hu, J. Li, S. Liu, Y. Lu, J. Niu, D. Tan, Y. Xu, T. Yan, Y. Zhong, F. Yan, X. Sun, and D. Yu, Scalable algorithm simplification using quantum and logic, *Nature Physics* **19**, 126 (2023).

[72] M. A. Nielsen and I. L. Chuang, *Quantum computation and quantum information* (Cambridge university press, 2010).

[73] Y. Yang, B. Yang, G. Ma, J. Li, S. Zhang, and C. T. Chan, Non-abelian physics in light and sound, *Science* **383**, eadf9621 (2024).

[74] S. Sun, X. Wang, S. Li, D. Zhang, Q.-D. Chen, and X.-L. Zhang, Reconfigurable non-abelian integrated photonics, *Nature Communications* **16**, 7089 (2025).